Advances in Atmospheric Sciences
Impact Factor: 5.8
E-alert
ISSN 0256-1530
CN 11-1925/O4

A 10-Year Dataset of Land Surface Observations for the Semi-Humid Alpine Grassland in the Source Region of the Yellow River

Xianhong MENG, Yu ZHANG, Lunyu SHANG, Shaoying WANG, Zhaoguo LI, Shihua LYU, Yinhuan AO, Siqiong LUO, Lijuan WEN, Lin ZHAO, Hao CHEN, Di MA, Suosuo LI, Lele SHU, Yingying AN, Danrui SHENG, Hanlin NIU, Mingshan DENG

Citation: Meng, X. H., and Coauthors 2025: A 10-Year Dataset of Land Surface Observations for the Semi-Humid Alpine Grassland in the Source Region of the Yellow River, *Adv. Atmos. Sci.*, 42, 1261-1272. doi: 10.1007/s00376-024-4054-5.

View online: https://doi.org/10.1007/s00376-024-4054-5

ADVANCES IN ATMOSPHERIC SCIENCES, VOL. 42, JUNE 2025, 1261–1272

• **Data Description Article** •

A 10-Year Dataset of Land Surface Observations for the Semi-Humid Alpine Grassland in the Source Region of the Yellow River※

Xianhong MENG[1,2], Yu ZHANG[3], Lunyu SHANG[*1,2], Shaoying WANG[*1,2], Zhaoguo LI[1,2], Shihua LYU[3], Yinhuan AO[1,2], Siqiong LUO[1,2], Lijuan WEN[1,2], Lin ZHAO[1,2], Hao CHEN[1,2], Di MA[1,2], Suosuo LI[1,2], Lele SHU[1,2], Yingying AN[1,2], Danrui SHENG[1,2,4], Hanlin NIU[1,2,4], and Mingshan DENG[1,2]

[1]*Key Laboratory of Cryospheric Science and Frozen Soil Engineering*, *Northwest Institute of Eco-Environment and Resources*, *Chinese Academy of Sciences*, *Lanzhou* 730000, *China*

[2]*Zoige Plateau Wetland Ecosystem Research Station*, *Northwest Institute of Eco-Environment and Resources*, *Chinese Academy of Sciences*, *Lanzhou* 730000, *China*

[3]*Plateau Atmosphere and Environment Key Laboratory of Sichuan Province*, *School of Atmospheric Sciences*, *Chengdu University of Information Technology*, *Chengdu* 610225, *China*

[4]*University of Chinese Academy of Sciences*, *Beijing* 100049, *China*

(Received 5 February 2024; revised 18 September 2024; accepted 8 October 2024)

ABSTRACT

The source region of the Yellow River, accounting for over 38% of its total runoff, is a critical catchment area, primarily characterized by alpine grasslands. In 2005, the Maqu land surface processes observational site was established to monitor climate, land surface dynamics, and hydrological variability in this region. Over a 10-year period (2010–19), an extensive observational dataset was compiled, now available to the scientific community. This dataset includes comprehensive details on site characteristics, instrumentation, and data processing methods, covering meteorological and radiative fluxes, energy exchanges, soil moisture dynamics, and heat transfer properties. The dataset is particularly valuable for researchers studying land surface processes, land–atmosphere interactions, and climate modeling, and may also benefit ecological, hydrological, and water resource studies. The report ends with a discussion on perspectives and challenges of continued observational monitoring in this region, focusing on issues such as cryosphere influences, complex topography, and ecological changes like the encroachment of weeds and scrubland.

Key words: field observation dataset, land surface processes, alpine grassland, energy and water exchanges, Yellow River source region, Tibetan Plateau

Citation: Meng, X. H., and Coauthors, 2025: A 10-year dataset of land surface observations for the semi-humid alpine grassland in the source region of the Yellow River. *Adv. Atmos. Sci.*, **42**(6), 1261−1272, https://doi.org/10.1007/s00376-024-4054-5.

Dataset Profile

Dataset title	A 10-Year Dataset of Land Surface Observations for the Semi-Humid Alpine Grassland in the Source Region of the Yellow River
Time range	January 2010–1 January 2020
Geographical scope	33°55′17″N, 102°09′03″E
Data format	".csv"
Data volume	36.3 MB
Data service system	https://www.doi.org/10.12072/ncdc.zpwers.db4092.2023, and https://www.scidb.cn/en/doi/10.12072/ncdc.zpwers.db4092.2023

※ This paper is a contribution to the special topic on Land Surface Processes Observations on the Source Region of the Yellow River.

* Corresponding authors: Lunyu SHANG, Shaoying WANG
Emails: sly@lzb.ac.cn, wangshaoying@lzb.ac.cn

(Continued.)

Dataset Profile	
Sources of Funding	National Natural Science Foundation of China for Distinguished Young Scholars (Grant No. 42325502), the 2nd Scientific Expedition to the Qinghai–Tibet Plateau (Grant No. 2019QZKK0102), the West Light Foundation of the Chinese Academy of Sciences (Grant No. xbzg-zdsys-202215), the Science and Technology Research Plan of Gansu Province (Grant Nos. 23JRRA654 and 20JR10RA070), the Youth Innovation Promotion Association of the Chinese Academy of Sciences (Grant No. QCH2019004), iLEAPS (integrated Land Ecosystem–Atmosphere Processes Study).
Dataset composition	The dataset contains a turbulent flux file named "Flux.csv", a meteorology file named "Meteorology.csv" and a soil file named "Soil.csv".

1. Introduction

The Source Region of the Yellow River (SRYR), covering approximately 12.2 × 10^4 km^2, is a key watershed for the Yellow River, contributing about 38% of its total runoff (Zhang et al., 2013). Known as "China's Water Tower", this region is essential for water resource security and sustainable development of the Yellow River Basin. The SRYR's climate varies, with the eastern part classified as semi-humid and the western part as semi-arid. The area is influenced by the East Asian and Indian monsoons, as well as the Westerlies, leading to a complex precipitation pattern (Hu et al., 2011; Qin et al., 2017). Recently, precipitation trends in the SRYR have diverged, with notable increases in the western semi-arid region and significant decreases in the eastern subhumid region (Liu et al., 2021).

The Zoige Plateau, situated in the eastern part of the SRYR, receives an average of 600–800 mm of precipitation annually and falls within the alpine subhumid climate zone. As the largest alpine peatland wetland in the world, the Zoige Plateau significantly impacts runoff dynamics, contributing 58.7% of the SRYR's total runoff and helping balance water availability during both wet and dry periods (Wang, 2008; Bai et al., 2013). The landscape, dominated by alpine grasslands and featuring lakes, marshes, and seasonally frozen soil, interacts with the atmosphere through energy and water exchanges. This region has faced notable wetland degradation in recent decades, with declining water storage observed from 1981 to 2011 (Lu et al., 2019). Until recently, however, in situ atmospheric and hydrological observations in the Zoige Plateau were limited, leaving gaps in understanding the hydroclimatic changes in the area.

As a vital part of the eastern Tibetan Plateau (TP), the Zoige Plateau represents a semi-humid zone. While datasets have been collected in other TP regions, long-term observational data from this semi-humid northeastern zone are scarce (Liu et al., 2011, 2018; Che et al., 2019; Ma et al., 2020). Addressing this gap is crucial for advancing land surface parameterizations, improving remote sensing validation, and understanding land surface processes more comprehensively.

In response, a land surface observation site was established in Maqu County, Gansu Province, in the heart of the Zoige Plateau. It was set up firstly in 2005, and became an official site in 2008, with more facilities added on over time for observing marsh wetlands, shrublands, and additional meteorological parameters. This site has since become a vital platform for studying land–atmosphere interactions, enabling advancements in ecohydrology, land surface modeling, and investigation of regional ecological processes (Luo et al., 2009; Shang et al., 2015; Wang et al., 2016; Wang et al., 2019; Deng et al., 2020, 2021; Li et al., 2021a; Li et al., 2021b; Wang et al., 2021; An et al., 2022).

This paper introduces a decade-long dataset (2010–19) from this site, aiming to address key scientific questions on land–atmosphere interactions. Section 2 provides an overview of the site's instruments and data; section 3 addresses data integrity; section 4 examines meteorological variables, radiation budgets, energy exchanges, and soil characteristics; and section 5 discuss the significance of the dataset. Finally, section 6 offers a summary and perspectives. The study contributes to the development of land surface models for cold regions and aims to enhance understanding of climate change, ecology, and water resource security in the SRYR.

2. Site, instruments and data descriptions

2.1. *Site information*

The Maqu observational site (33°55'17"N, 102°09'03"E, 3434 m above sea level), located in Maqu County, southwest Gansu Province, China, was established in 2005 by the Zoige Plateau Wetland Ecosystem Research Station, which is part of the Northwest Institute of Eco-Environment and Resources, Chinese Academy of Sciences. Data from the Maqu meteorological station indicate that the average air temperature in the area from 1981 to 2020 was 2.1°C, with an annual average precipitation of 608.7 mm. The site features a typical alpine grassland with seasonal frozen soil, characterized by a flat terrain covered with meadows reaching heights of 0.2 m in summer and 0.1 m in winter. Soil texture details for the shallow soil are provided in Table 1, and the observational site and its environment are depicted in Fig. 1.

2.2. *Instruments and data processing*

The sensors installed at the Maqu site are detailed in Table 2. EddyPro 6.0 software from LI-COR Biosciences in Lincoln, NE, USA, was utilized to calculate 30-min sensible heat flux and latent heat flux from raw data collected at 10 Hz. The processing of the EC data involved removing spikes (Vickers and Mahrt, 1997), double coordinate rotation (Wilczak et al., 2001), compensation for density fluctuations

Table 1. Soil texture of the Maqu site.

Depth (m)	Organic matter (g kg^{-1})	Gravel (%)	Sand (%)					Silt (%)	Clay (%)
		> 2 mm	2–1 mm	1–0.5 mm	0.5–0.25 mm	0.25–0.1 mm	0.1–0.05 mm	0.05–0.002 mm	< 0.002 mm
0.05	35.96	0	0	3.12	19.873	46.328	21.091	9.588	0
0.1	35.41	0	0	4.347	16.685	46.627	22.554	9.787	0
0.2	16.30	0.449	0	0	7.359	50.512	26.085	15.417	0.627
0.4	16.45	2.331	0	0	7.513	47.485	24.999	18.991	1.012

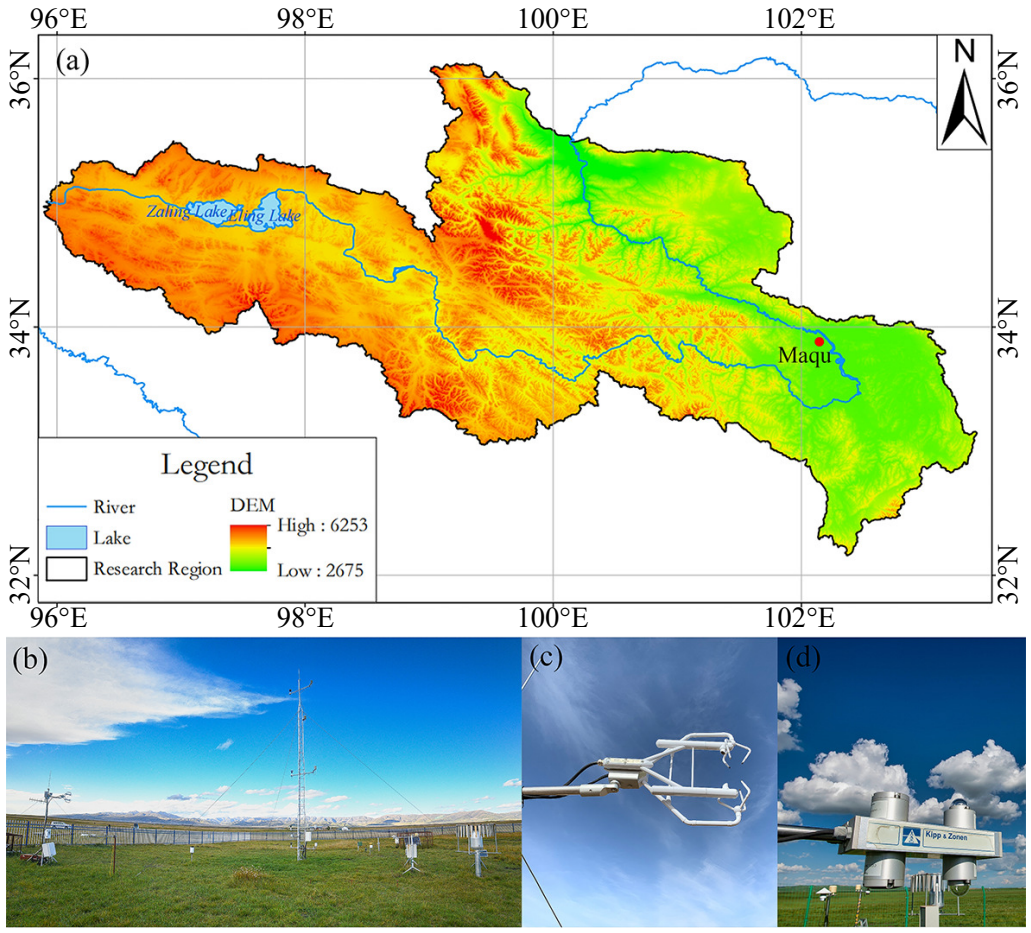

Fig. 1. (a) Digital elevation map and climatic conditions of the SRYR, with the location of the observational site marked by the red spot. (b) Condition of the observation site. (c) 3D sonic anemometer and gas analyzer sensors. (d) Radiation sensor.

Table 2. Sensors used at the Maqu site.

Variable	Sensor (s)	Manufacturer	Period	Height (s)	Units
Air temperature	HMP45C	Vaisala	2010–19	2.75 m	°C
Relative humidity					%
Wind speed	CSAT3	Campbell	2010–19	2.75 m	m s^{-1}
Wind direction					°
Atmospheric pressure	PTB110	Vaisala	2010–19	1 m	kPa
Radiation flux	CNR1	Kipp&Zonen	2010–19	1.5 m	W m^{-2}
Sensible and latent heat flux	CSAT3	Campbell	2010–19	2.75 m	W m^{-2}
	Li-7500	Li-Cor	2010–11		
	EC150	Campbell	2012–19		
Precipitation	52202	Young	2010–11	1.5 m	mm
	TE525MM	Texas Electronics	2012–19		
Soil temperature	109SS	Campbell	2010–19	0.05/0.10/0.20/0.40 m	°C
Soil moisture	CS616	Campbell	2010–19	0.05/0.10/0.20/0.40 m	m^3 m^{-3}

(Webb et al., 1980), and frequency response correction (Moncrieff et al., 1997). Then, the 30-min flux data were filtered for (1) incomplete 30-min measurements, (2) low quality due to insufficient turbulence and non-steady state (Mauder and Foken, 2004), (3) outliers (Papale et al., 2006), and (4) H_2O signal strength lower than 0.8. Following that, around 23% of sensible heat flux data and 26% of latent heat flux data gathered between 2010 and 2019 were not recorded. Afterwards, the missing sensible and latent heat flux data were completed by utilizing the marginal distribution sampling technique (Reichstein et al., 2005) in the R package REddyproc (Wutzler et al., 2018).

2.3. *Data availability*

The data variables were extracted and saved as csv files (Flux.csv, Meteorology.csv, Soil.csv). The data files use Beijing time (UTC+8) and have been made available for download at the National Cryosphere Desert Data Center (https://www.doi.org/10.12072/ncdc.zpwers.db4092.2023) and Science Data Bank (https://www.scidb.cn/en/doi/10.12072/ncdc.zpwers.db4092.2023).

3. Data integrity

Figures 2–5 provide a summary of key characteristics and statistics for the half-hourly variables monitored annually. An almost complete dataset is available for all meteorological variables except precipitation, which has an overall missing rate of 14.2% over the 10-year period. The highest levels of missing precipitation data occur in 2012 and 2013 (Fig. 2). Shortwave radiation fluxes have a slightly lower missing rate (1.8%) compared to longwave radiation fluxes (2.4%) (Fig. 3). The calculated net radiation flux also shows a missing rate of 2.4% over the decade.

Regarding soil hydrothermal observations, the soil temperature data are generally more complete than the soil moisture data. The largest gaps in soil temperature are 8.8% at the depth of 10 cm in 2015 and 7.1% at the depth of 20 cm in 2019. Soil moisture data across four layers have a missing rate of approximately 1%, with continuous data from 2013 to 2019. For soil heat flux, the overall missing rate is 2.5%, with higher rates in 2011 (12.6%) and 2019 (7.1%).

The original dataset of turbulent heat fluxes have notable gaps, with approximately 77% and 74% data availability for sensible and latent heat fluxes over the 10-year period, respectively. The largest data gaps in these fluxes are between 2010 and 2013, particularly in 2012. These gaps have been amended using the gap-filling method detailed in section 2.2. In Fig. 5, the gap-filled data, repre-

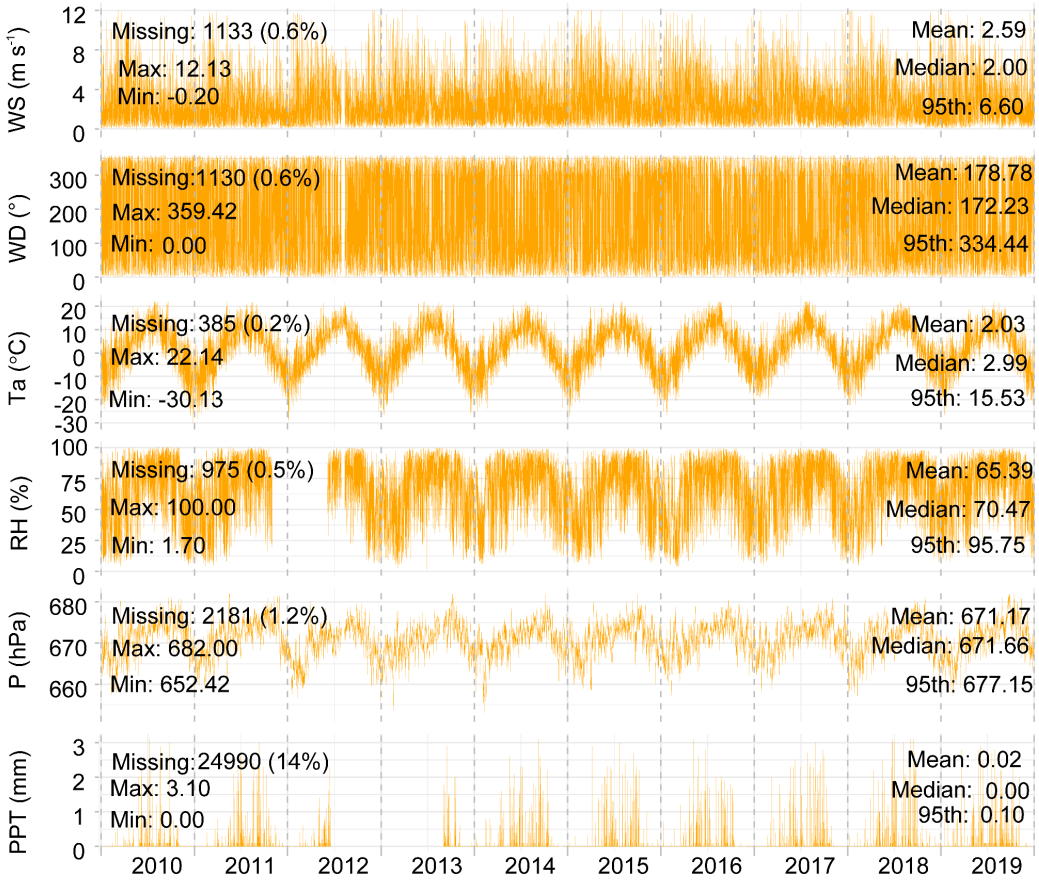

Fig. 2. Statistical characteristics of gaps in wind speed (WS, m s^{-1}), wind direction (WD, °), air temperature (Ta, °C), relative humidity (RH, %), atmospheric pressure (P, hPa), and precipitation (PPT, mm), from 2010 to 2019, based on observations at 30-min intervals. The word "missing" indicates the amount and percentage (in brackets) of total missing data. Information on the min, max, mean, median and 95th percentile is also shown in the figure.

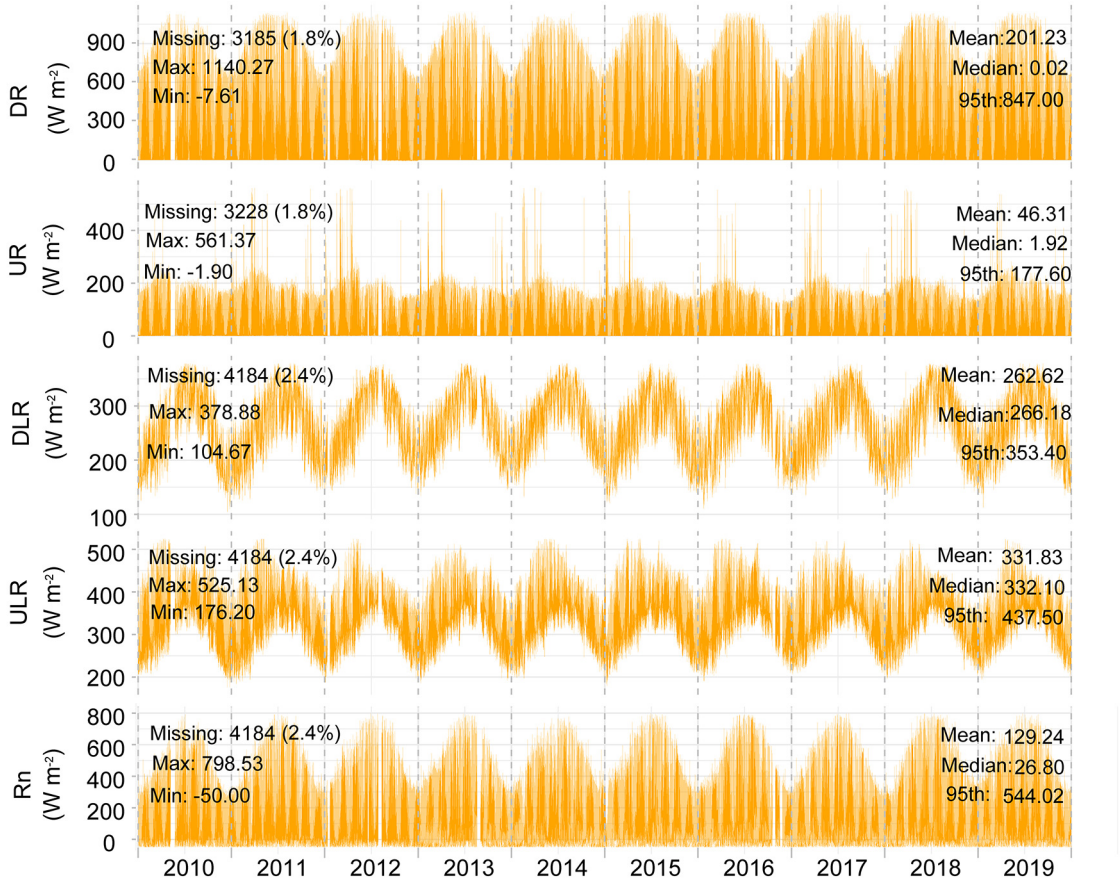

Fig. 3. As in Fig. 2 but for downward shortwave radiation (DR, W m^{-2}), upward shortwave radiation (UR, W m^{-2}), downward longwave radiation (DLR, W m^{-2}), upward longwave radiation (ULR, W m^{-2}), and net radiation (Rn, W m^{-2}).

sented by blue lines, are displayed alongside the original data, highlighting areas with significant data completion efforts. The gap-free data have been assigned a data quality indicator of 0 in the flux file.

4. Basic characteristics of the observations

4.1. *Meteorological observations*

To ascertain the fundamental characteristics of land surface processes, monthly average diurnal cycles are derived by averaging half-hourly data, and daily data are produced as daily averages from the half-hourly data. Figure 6 illustrates seasonal variations in monthly average diurnal cycles and daily average values of air temperature, atmospheric pressure, relative humidity, and wind speed. Over the 10-year period, the average air temperature at the site is 2.1°C, with extreme half-hourly values ranging from 25.6°C to −30.1°C. The highest daily average temperature (12.8°C) occurs in early August, while the lowest recorded (−13.1°C) is in early January. Throughout the year, atmospheric pressure shows a pattern of an increase from March to October, followed by a decrease until February, with two peaks annually corresponding to climate and vegetation conditions. The maximum daily average atmospheric pressure recorded is 676.7 hPa, the minimum is 663.8 hPa, and the average is 671.2 hPa, with most values falling within the range of 665 to 675 hPa. Daily average relative humidity ranges from 37.6% to 83.6%, with an average of 65.4%. Relative humidity consistently exceeds 60% from May to October. The maximum half-hourly wind speed observed is 16.3 m s^{-1}, with daily averages typically below 4 m s^{-1}. Wind speed peaks in winter and spring and decreases during summer and autumn, showing significant daily fluctuations.

4.2. *Radiation flux observations*

Figure 7 illustrates seasonal fluctuations of monthly average diurnal cycles and daily average radiation fluxes. The average downward shortwave radiation recorded is 202.2 W m^{-2}, with the extreme half-hourly value reaching 1380 W m^{-2}. The daily average downward shortwave radiation exhibits an upward trend from January to April, followed by a decline from May to June, a subsequent rise in July, and a decrease for the remainder of the year. The peak daily average downward shortwave radiation (309.1 W m^{-2}) occurs in August, with the highest value of 849.5 W m^{-2} in April. Upward shortwave radiation follows a similar seasonal pattern to downward shortwave radiation, peaking at 95.9 W m^{-2} in April due to vegetation and snowfall conditions. Downward longwave radiation and upward longwave

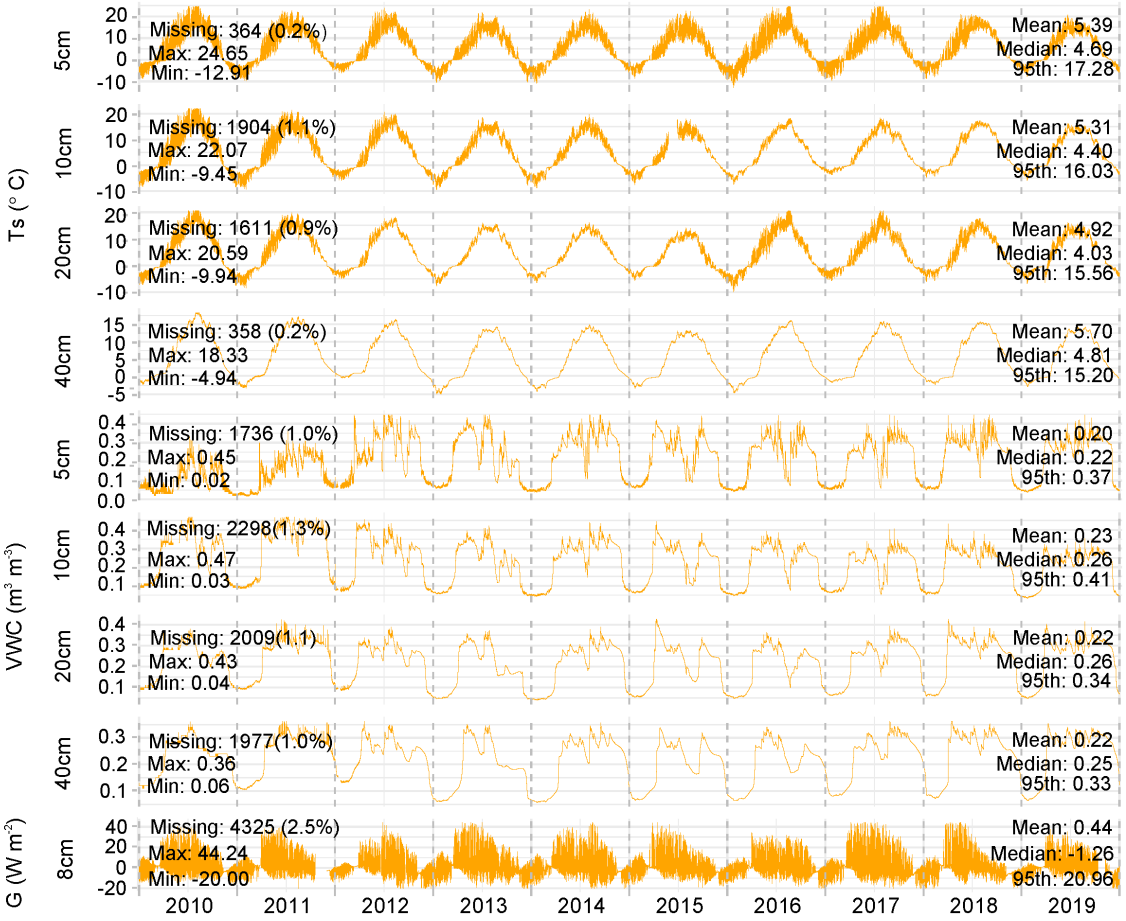

Fig. 4. As in Fig. 2 but for soil temperature (Ts, °C) and soil moisture (VWC, m^3 m^{-3}) at depths of 5, 10, 20 and 40 cm, and soil heat flux (G, W m^{-2}) at a depth of 8 cm.

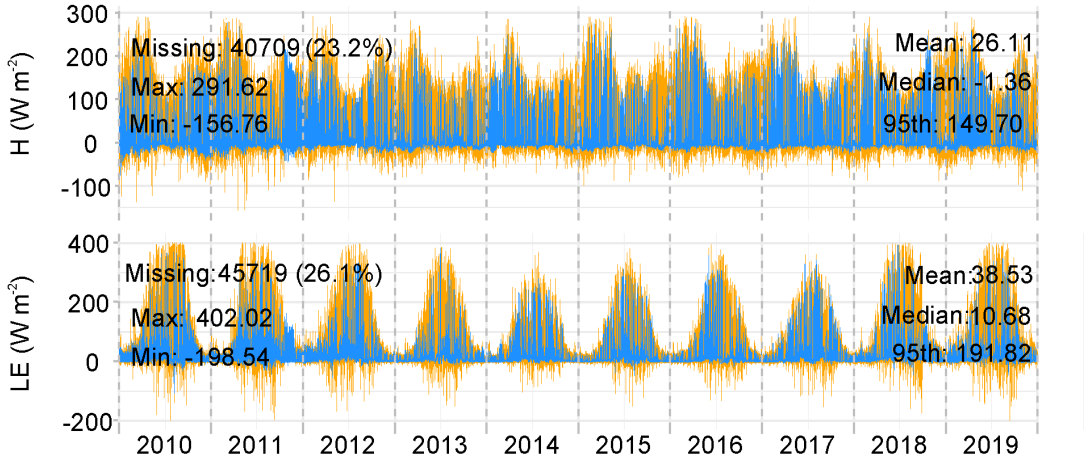

Fig. 5. As in Fig. 2 but for sensible heat flux (H, W m^{-2}) and latent heat flux (LE, W m^{-2}). The orange lines represent the original data with gaps and the blue lines represent the gap-filled data.

radiation exhibit parallel seasonal variations. However, since it is a 10-year monthly average diurnal cycle, the values are not continuous for each month. Both downward and upward longwave radiation daily averages increase from January to July and decrease from August to December. The peak daily average values for downward and upward longwave radiation are 363.3 and 361.7 W m^{-2}, respectively.

4.3. *Soil hydrothermal observations*

Figure 8 illustrates the seasonal fluctuations in monthly average diurnal cycles and daily mean levels of soil temperature and soil moisture at various depths. Both soil temperature and moisture show significant seasonal variations, with soil temperature peaking during the summer months and soil mois-

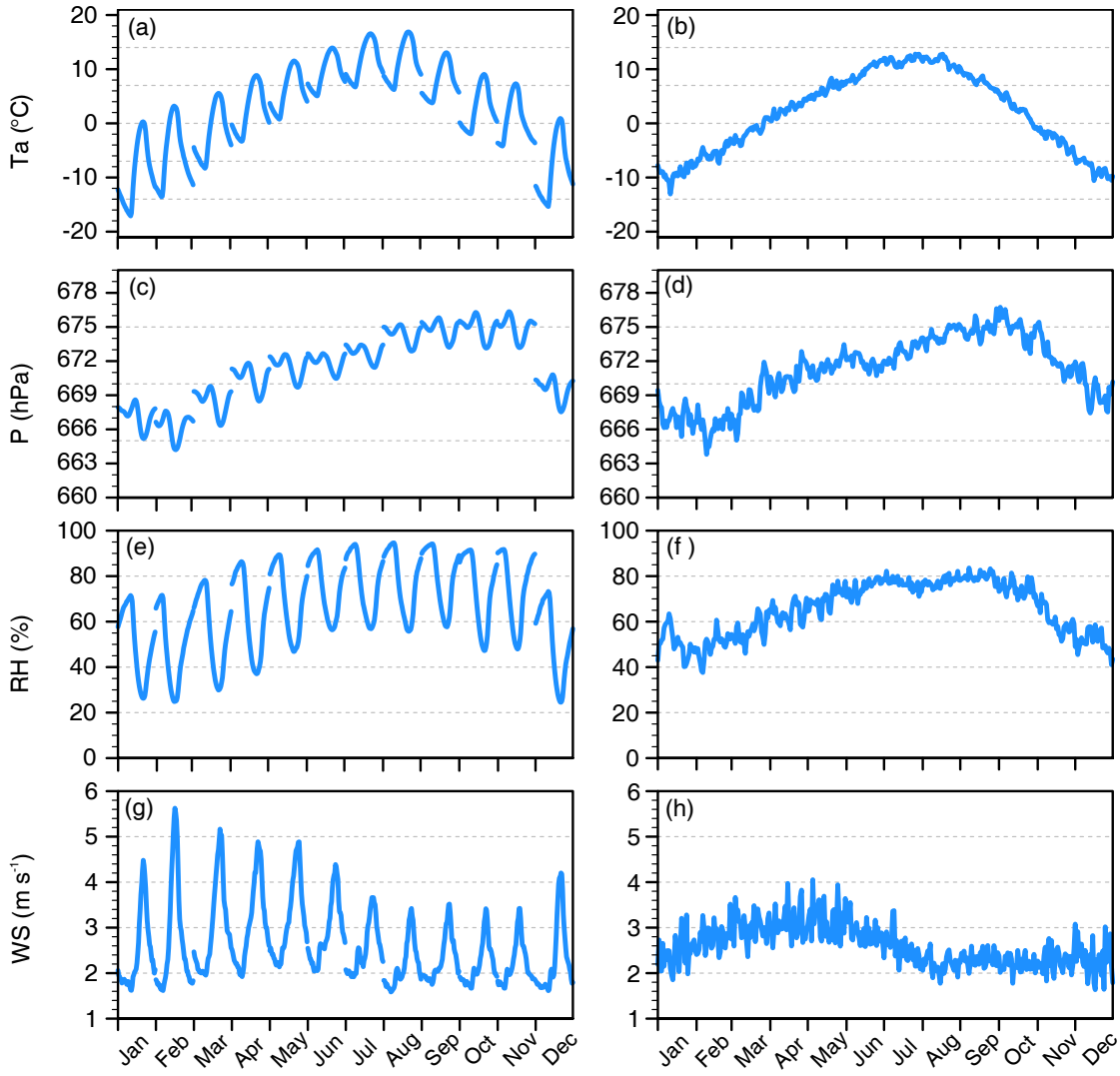

Fig. 6. Seasonal variations of monthly average diurnal cycles (left column) and daily average values (right column) of air temperature (Ta, °C), atmospheric pressure (P, hPa), relative humidity (RH, %), and wind speed (WS, m s^{-1}).

ture maintaining relatively high levels across all layers from April to early November, which is the non-freezing period for the soil. The average daily soil temperature values recorded at the depths of 5, 10, 20 and 40 cm are 5.4°C, 5.3°C, 4.9°C and 5.7°C, respectively, with the highest half-hourly soil temperature reaching 27.7°C at the depth of 5 cm. Soil temperature fluctuations are more pronounced in the shallower layers and exhibit drier conditions in the deeper layers. Daily mean soil moisture values measured at the depths of 5, 10, 20 and 40 cm are 0.20, 0.23, 0.22 and 0.22 m^3 m^{-3}, respectively. However, the soil moisture probability distribution depicted in Fig. 4 indicates that a greater number of values fall within the range of 0.25–0.30 m^3 m^{-3} at the depths of 20 and 40 cm, while most values remain below 0.3 m^3 m^{-3} at the depth of 10 cm.

4.4. *Turbulent flux observations*

Figure 9 illustrates the seasonal fluctuations in the monthly average diurnal cycles and daily average values of sensible and latent heat flux. Sensible heat flux exhibits minimal variability, whereas latent heat flux displays significant fluctuations over the course of the year. The mean sensible heat flux recorded for the location over the decade is 31.4 W m^{-2}, with daily averages ranging from 13.5 to 50.6 W m^{-2}. Sensible heat flux shows an upward trend from January to April, followed by a decline from May to June, and subsequently fluctuates within a lower range from July to December. The highest and lowest daily average sensible heat flux values are in late March and early July, respectively. On the other hand, the average latent heat flux for the site calculated over the same 10-year period is 46.8 W m^{-2}, with daily averages ranging from 5.8 to 91.8 W m^{-2}. Latent heat flux exhibits an ascending pattern from January, peaking in early August, and then declining for the remainder of the year. The peak diurnal sensible heat flux (164.0 W m^{-2}) and latent heat flux (241.7 W m^{-2}) recorded are in March and August, respectively. Notably, during the growing season (May to September), the daily average latent heat flux

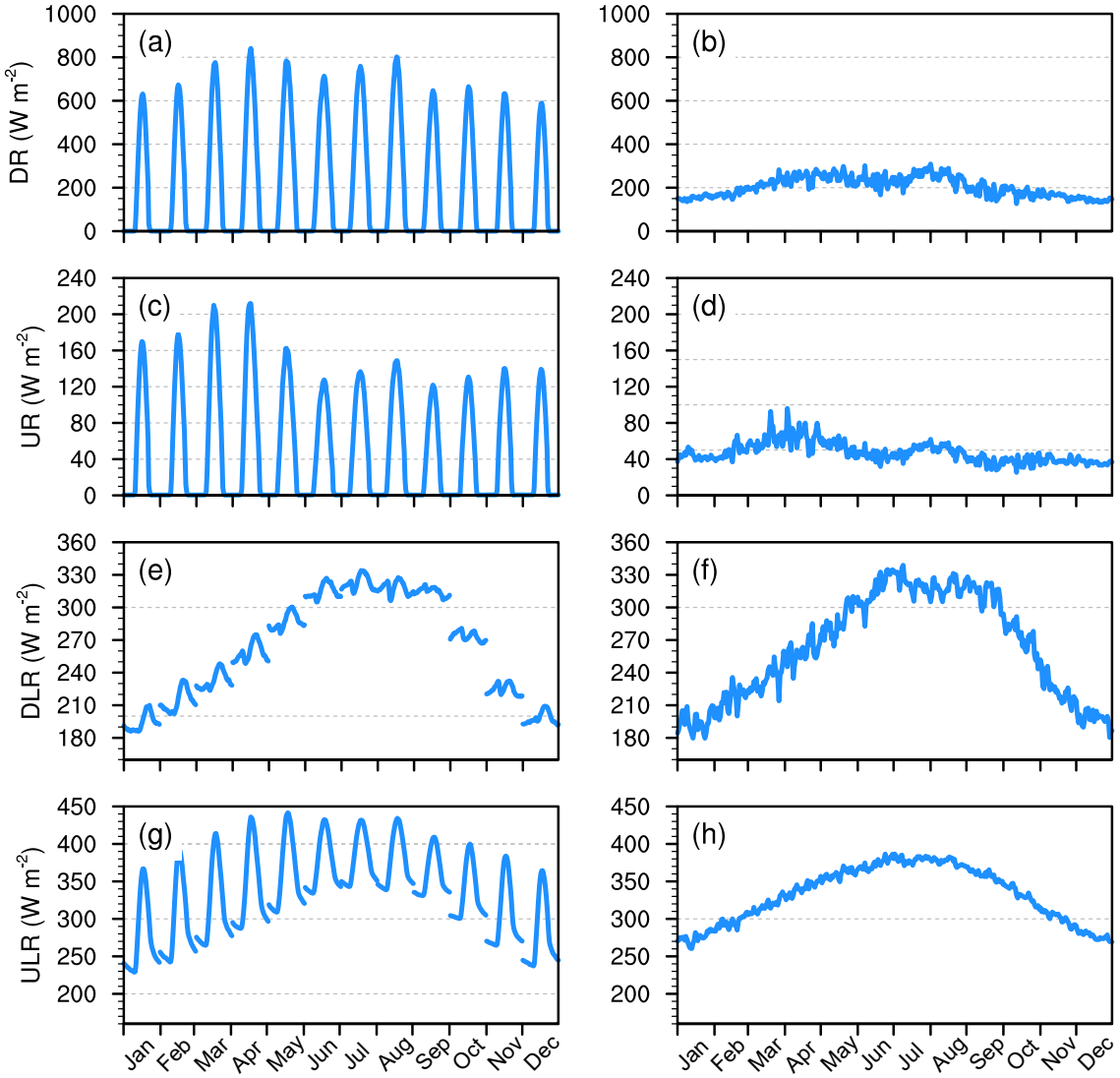

Fig. 7. As in Fig. 6 but for downward shortwave radiation (DR, W m^{-2}), upward shortwave radiation (UR, W m^{-2}), downward long wave radiation (DLR, W m^{-2}), and upward long wave radiation (ULR, W m^{-2}).

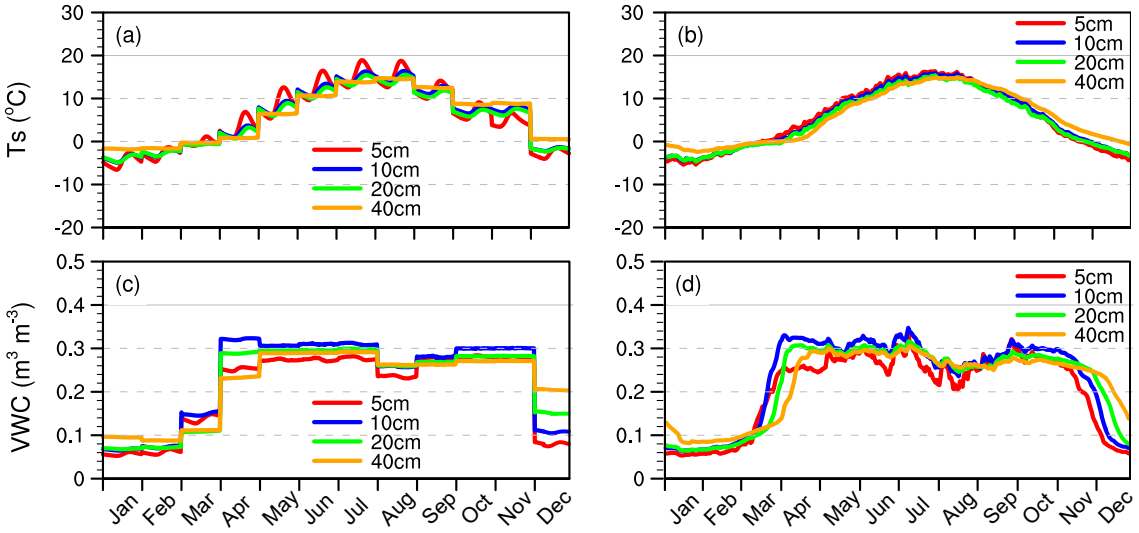

Fig. 8. As in Fig. 6 but for soil moisture (VWC, m^3 m^{-3}) and soil temperature (Ts, °C) at the depths of 5, 10, 20 and 40 cm.

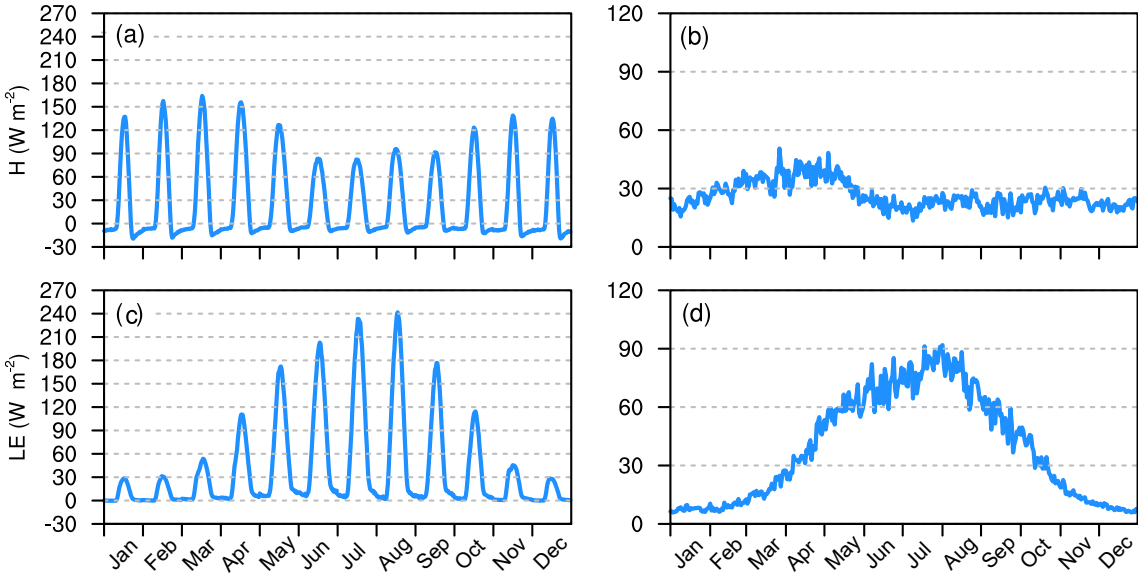

Fig. 9. As in Fig. 6 but for sensible heat flux (H, W m^{-2}) and latent heat flux (LE, W m^{-2}).

exceeds the daily average sensible heat flux, indicating that latent heat flux is the primary consumer of surface available energy during this period. This trend persists throughout the growing season, emphasizing the dominance of latent heat flux in consuming surface available energy.

5. Discussion

This site, representing a typical subhumid climate zone, is a valuable location for studying common surface conditions on the TP. In comparison to previous observations conducted over the TP by Liu et al. (2011, 2018), Che et al. (2019), and Ma et al. (2020), the average albedo recorded during the growing season is the lowest, at 0.19, due to the abundant vegetation cover. The average Bowen ratio (the ratio of sensible to latent heat flux) during the growing season is 0.57, which is only surpassed by forested areas on the TP. This underscores the significance and representativeness of this site for the alpine grassland underlying surface in the subhumid region of the TP.

Based on the collected data, seasonal data allowed for the calculation of soil thermal conductivity values, recorded at 0.27, 0.38, 0.55 and 0.83 W m^{-1} K^{-1} for spring, summer, autumn and winter, respectively, with variations attributed to soil ice content changes. Additional parameters, such as aerodynamic roughness length, zero plane displacement, soil hydraulic conductivity, and snow thermal conductivity were also derived, informing iterative improvements to physical parameterization. Notably, Luo et al. (2009) refined the soil thermal conductivity model using field data, with subsequent updates by Chen et al. (2014) on soil organic matter impacts. Deng et al. (2020) further evaluated soil temperature and moisture simulations based on observations from this and other TP sites, leading to a more generalized parameterization scheme for land surface processes across the TP.

Alpine grassland plays an essential role in water conservation because of its ecological functions. Recent work by Deng et al. (2022) advanced the parameterization of seasonal –deciduous phenology in grasslands using the Community Land Surface Biogeochemical Dynamic Vegetation Model, achieving more accurate simulations of gross primary productivity. Their model, which explored climate warming impacts on vegetation and runoff in the Three Rivers Source Region, indicated a 33% reduction in runoff from 1980 to 2016 due to vegetation changes (Deng et al., 2023), underscoring alpine grassland's significance in regional water conservation.

In addition to validating models and remote sensing products, it is crucial to monitor how land surface processes respond to climatic or meteorological events. Figure 10 illustrates the annual fluctuations of meteorological factors during both the growing and non-growing seasons. Notably, significant disparities in these variables between these two distinct periods are evident. The notably low precipitation levels in 2015 align with the broader trend of extreme aridity on the TP during El Niño, as discussed in prior research (Lei et al., 2019), coinciding with extreme values of soil moisture and sensible heat flux. Over the period from 2012 to 2017, precipitation exhibited a fluctuating pattern featuring a decrease followed by an increase, mirroring corresponding variations in sensible and latent heat fluxes. Moreover, while there were no significant precipitation variations during the non-growing season and there was a substantial disturbance in sensible heat flux during this period—a trend that was only discernible through long-term monitoring efforts. Ongoing observations at this site will continue to extend these valuable time-series data.

6. Summary and outlook

This paper provides an overview of a decade-long dataset of land surface observations collected from alpine

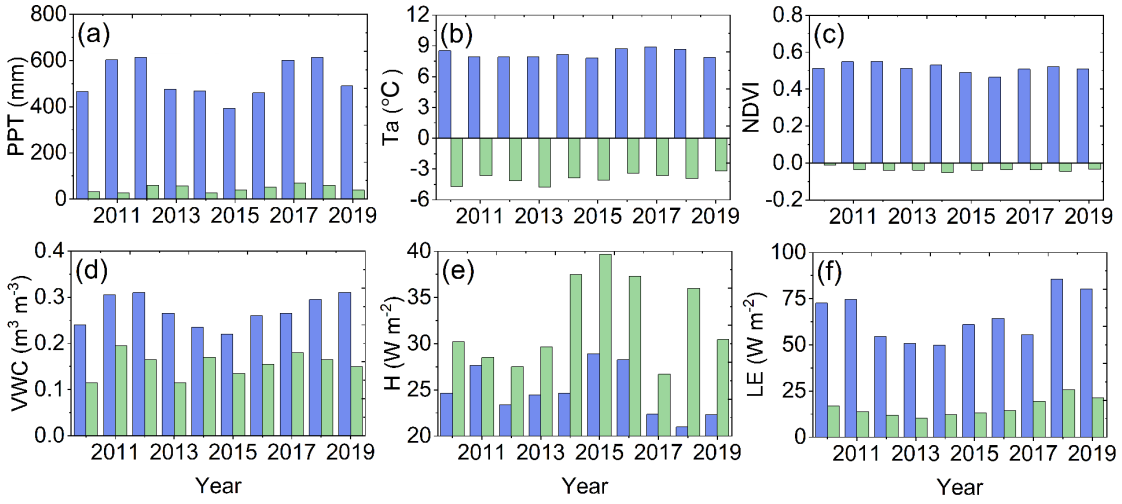

Fig. 10. Annual changes in average cumulative precipitation (PPT, mm yr^{-1}), 2-m air temperature (Ta, °C), NDVI, soil water content (VWC, m^3 m^{-3}), sensible heat flux (H, W m^{-2}), and latent heat flux (LE, W m^{-2}) in the growing and non-growing season. The blue bar is for growing season, and the green bar is for non-growing season.

grassland in the SRYR. As this area becomes increasingly significant in the context of climate change, there is an urgent need for observational data to support research on the regional hydrological cycle, water resources, and ecosystem response. The primary aim of this report is to emphasize the dataset's availability and offer a foundational reference point. In this instance, we present observations that can be structured to exhibit a greater degree of continuity prior to 2019, although data from 2005 to 2009 are relatively limited owing to maintenance challenges. We also plan to organize and disseminate data collected after 2019, which will be accessible through the same data URL used for this release. By making this dataset available, we hope to enhance understanding and monitoring of this vital water system and its anticipated changes.

The dataset has facilitated research on various aspects, including the land surface radiation budget, energy partitioning, soil freeze–thaw cycles, and evaluation and development of land surface models and remote sensing products since the establishment of the observational system (Luo et al., 2009; Shang et al., 2015; Wang et al., 2016; Wang et al., 2019; Deng et al., 2020, 2021; Li et al., 2021a; Li et al., 2021b; Wang et al., 2021; An et al., 2022). The region has undergone notable changes, such as a retreat of the cryosphere and the encroachment of weeds and scrubland, which are attributed to climate warming. These changes impact the ecological system, hydrology, and water resources, highlighting the complex interactions between freeze–thaw processes and vegetation dynamics in mountainous regions. These dynamics influence land surface processes and contribute to feedback mechanisms within regional climate and hydrological cycles.

In light of these challenges, there is a need for a more sophisticated and integrated Earth system observing framework. To address this, we are developing an integrated observing system for land surface processes and hydrological–ecological interactions at the grassland site, alongside similar sites in scrubby watersheds. This initiative aims to facilitate interdisciplinary research on the atmosphere, land surface processes, and ecohydrology of the region, as well as their combined impacts.

Acknowledgements. This study was supported by the National Natural Science Foundation of China for Distinguished Young Scholars (Grant No. 42325502), the 2nd Scientific Expedition to the Qinghai–Tibet Plateau (Grant No. 2019QZKK0102), the West Light Foundation of the Chinese Academy of Sciences (Grant No. xbzg-zdsys-202215), the Science and Technology Research Plan of Gansu Province (Grant Nos. 23JRRA654 and 20JR10RA070), the Youth Innovation Promotion Association of the Chinese Academy of Sciences (Grant No. QCH2019004), iLEAPS (integrated Land Ecosystem–Atmosphere Processes Study). Thanks to all the scientists, engineers, students, and other people who participated in the field observations, instrument maintenance, and data processing.

REFERENCES

An, Y. Y., X. H. Meng, L. Zhao, Z. G. Li, S. Y. Wang, L. Y. Shang, H. Chen, and S. Lyu, 2022: Evaluation of surface albedo over the Tibetan Plateau simulated by CMIP5 models using in-situ measurements and MODIS. *International Journal of Climatology*, **42**(2), 928–951, https://doi.org/10.1002/joc.7281.

Bai, J. H., Q. Q. Lu, Q. Q. Zhao, J. J. Wang, and H. Ouyang, 2013: Effects of alpine wetland landscapes on regional climate on the Zoige Plateau of China. *Advances in Meteorology*, **2013**, 972430, https://doi.org/10.1155/2013/972430.

Che, T., and Coauthors, 2019: Integrated hydrometeorological, snow and frozen-ground observations in the alpine region of the Heihe River Basin, China. *Earth System Science Data*, **11**, 1483–1499, https://doi.org/10.5194/essd-11-1483-2019.

Chen B. L., S. Q. Luo, S. H. Lü, Y. Zhang, D. Ma, 2014: Effects of the soil freeze–thaw process on the regional climate of the Qinghai-Tibet Plateau. *Climate Research*, **59**, 243–257, https://doi.org/10.3354/cr01217.

Deng, M. S., X. H. Meng, Y. Lyv, L. Zhao, Z. G. Li, Z. Y. Hu, and H. Jing, 2020: Comparison of soil water and heat transfer modeling over the Tibetan Plateau using two Community Land Surface Model (CLM) versions. *Journal of Advances in Modeling Earth Systems*, **12**(10), e2020MS002189, https://doi.org/10.1029/2020MS002189.

Deng, M. S., and Coauthors, 2021: Impact and sensitivity analysis of soil water and heat transfer parameterizations in Community Land Surface Model on the Tibetan Plateau. *Journal of Advances in Modeling Earth Systems*, **13**(9), e2021MS002670, https://doi.org/10.1029/2021MS002670.

Deng, M. S., and Coauthors, 2022: The response of vegetation to regional climate change on the tibetan plateau based on remote sensing products and the dynamic global vegetation model. *Remote Sensing*, **14**, 3337, https://doi.org/10.3390/rs14143337.

Deng, M. S., and Coauthors, 2023: Impact of climatic and vegetation dynamic change on runoff over the Three Rivers Source Region based on the Community Land Model. *Climate Dyn.*, **61**, 1193–1208, https://doi.org/10.1007/s00382-022-06619-0.

Hu, Y. R., S. Maskey, S. Uhlenbrook, and H. L. Zhao, 2011: Streamflow trends and climate linkages in the source region of the Yellow River, China. *Hydrological Processes*, **25**(22), 3399–3411, https://doi.org/10.1002/hyp.8069.

Lei, Y. B., Y. L. Zhu, B. Wang, T. D. Yao, K. Yang, X. W. Zhang, J. Q. Zhai, and N. Ma, 2019: Extreme lake level changes on the Tibetan Plateau associated with the 2015/2016 El Niño. *Geophys. Res. Lett.*, **46**, 5889–5898, https://doi.org/10.1029/2019GL081946.

Li, G. W., X. H. Meng, E. Blyth, H. Chen, L. L. Shu, Z. G. Li, L. Zhao, and Y. S. Ma, 2021a: Impact of fully coupled hydrology-atmosphere processes on atmosphere conditions: Investigating the performance of the WRF-Hydro model in the Three River source region on the Tibetan Plateau, China. *Water*, **13**(23), 3409, https://doi.org/10.3390/w13233409.

Li, Z. G., S. Lyu, H. Chen, Y. H. Ao, L. Zhao, S. Y. Wang, S. B. Zhang, and X. H. Meng, 2021b: Changes in climate and snow cover and their synergistic influence on spring runoff in the source region of the Yellow River. *Science of the Total Environment*, **799**, 149503, https://doi.org/10.1016/j.scitotenv.2021.149503.

Liu, C. H., P. L. Wang, T. T. Wen, D. Yu, and W. R. Bai, 2021: Spatio-temporal characteristics of climate change in the Yellow River source area from 1960 to 2019. *Arid Zone Research*, **38**(2), 293–302, https://doi.org/10.13866/j.azr.2021.02.01. (in Chinese with English abstract)

Liu, S. M., Z. W. Xu, W. Z. Wang, Z. Z. Jia, M. J. Zhu, J. Bai, and J. M. Wang, 2011: A comparison of eddy-covariance and large aperture scintillometer measurements with respect to the energy balance closure problem. *Hydrology and Earth System Sciences*, **15**(4), 1291–1306, https://doi.org/10.5194/hess-15-1291-2011.

Liu, S. M., and Coauthors, 2018: The Heihe integrated observatory network: A basin-scale land surface processes observatory in China. *Vadose Zone Journal*, **17**(1), 1–21, https://doi.org/10.2136/vzj2018.04.0072.

Lu, H. Y., Z. W. Li, X. Y. Hu, and G. A. Yu, 2019: Estimation of runoff change and water storage in Zoige Plateau. *Journal of Water Resources and Water Engineering*, **30**(6), 12–19, https://doi.org/10.11705/j.issn.1672-643X.2019.06.03. (in Chinese with English abstract)

Luo, S. Q., S. H. Lü, and Y. Zhang, 2009: Development and validation of the frozen soil parameterization scheme in Common Land Model. *Cold Regions Science and Technology*, **55**(1), 130–140, https://doi.org/10.1016/j.coldregions.2008.07.009.

Ma, Y. M., and Coauthors, 2020: A long-term (2005–2016) dataset of hourly integrated land–atmosphere interaction observations on the Tibetan Plateau. *Earth System Science Data*, **12**, 2937–2957, https://doi.org/10.5194/essd-12-2937-2020.

Mauder, M., and T. Foken, 2004: Documentation and instruction manual of the eddy covariance software package TK2. Universität Bayreuth, Abt. Mikrometeorologie: Bayreuth, Germany.

Moncrieff, J. B., and Coauthors, 1997: A system to measure surface fluxes of momentum, sensible heat, water vapour and carbon dioxide. *J. Hydrol.*, **188–189**, 589–611, https://doi.org/10.1016/S0022-1694(96)03194-0.

Papale, D., and Coauthors, 2006: Towards a standardized processing of Net Ecosystem Exchange measured with eddy covariance technique: Algorithms and uncertainty estimation. *Biogeosciences*, **3**(4), 571–583, https://doi.org/10.5194/bg-3-571-2006.

Qin, Y., D. W. Yang, B. Gao, T. H. Wang, J. S. Chen, Y. Chen, Y. H. Wang, and G. H. Zheng, 2017: Impacts of climate warming on the frozen ground and eco-hydrology in the Yellow River source region, China. *Science of the Total Environment*, **605–606**, 830–841, https://doi.org/10.1016/j.scitotenv.2017.06.188.

Reichstein, M., and Coauthors, 2005: On the separation of net ecosystem exchange into assimilation and ecosystem respiration: Review and improved algorithm. *Global Change Biology*, **11**(9), 1424–1439, https://doi.org/10.1111/j.1365-2486.2005.001002.x.

Shang, L. Y., Y. Zhang, S. H. Lü, and S. Y. Wang, 2015: Energy exchange of an alpine grassland on the eastern Qinghai-Tibetan Plateau. *Science Bulletin*, **60**, 435–446, https://doi.org/10.1007/s11434-014-0685-8.

Vickers, D., and L. Mahrt, 1997: Quality control and flux sampling problems for tower and aircraft data. *J. Atmos. Oceanic Technol.*, **14**(3), 512–526, https://doi.org/10.1175/1520-0426(1997)014<0512:QCAFSP>2.0.CO;2.

Wang, J. Y., S. Q. Luo, Z. G. Li, S. Y. Wang, and Z. H. Li, 2019: The freeze/thaw process and the surface energy budget of

the seasonally frozen ground in the source region of the Yellow River. *Theor. Appl. Climatol.*, **138**(3–4), 1631–1646, https://doi.org/10.1007/s00704-019-02917-6.

Wang, S. Y., Y. Zhang, S. H. Lü, P. X. Su, L. Y. Shang, and Z. G. Li, 2016: Biophysical regulation of carbon fluxes over an alpine meadow ecosystem in the eastern Tibetan Plateau. *International Journal of Biometeorology*, **60**(6), 801–812, https://doi.org/10.1007/s00484-015-1074-y.

Wang, W. H., 2008: Strategy of ecological protection for water source supply areas of the Yellow River in southern Gansu Province. *Yangtze River*, **39**, 25–27, https://doi.org/10.3969/j.issn.1001-4179.2008.20.009.

Wang, Y. Y., and Coauthors, 2021: Carbon fluxes and environmental controls across different alpine grassland types on the Tibetan Plateau. *Agricultural and Forest Meteorology*, **311**, 108694, https://doi.org/10.1016/j.agrformet.2021.108694.

Webb, E. K., G. I. Pearman, and R. Leuning, 1980: Correction of flux measurements for density effects due to heat and water vapour transfer. *Quart. J. Roy. Meteor. Soc.*, **106**(447), 85–100, https://doi.org/10.1002/qj.49710644707.

Wilczak, J. M., S. P. Oncley, and S. A. Stage, 2001: Sonic anemometer tilt correction algorithms. *Bound.-Layer Meteorol.*, **99**(1), 127–150, https://doi.org/10.1023/A:1018966204465.

Wutzler, T., A. Lucas-Moffat, M. Migliavacca, J. Knauer, K. Sickel, L. Šigut, O. Menzer, and M. Reichstein, 2018: Basic and extensible post-processing of eddy covariance flux data with REddyProc. *Biogeosciences*, **15**(16), 5015–5030, https://doi.org/10.5194/bg-15-5015-2018.

Zhang, Y., Y. F. Fu, and B. X. Hou, 2013: Analysis of the causes for runoff evolulation in the Yellow River source region. *Yellow River*, **35**(8), 22–24, https://doi.org/10.3969/j.issn.1000-1379.2013.08.007. (in Chinese with English abstract)